

Collective excitations induced by pairing anti-halo effect

Masayuki Yamagami^{1,2}

¹*Heavy Ion Nuclear Physics Laboratory, RIKEN, Hirosawa 2-1, Wako, Saitama 351-0198, Japan*

²*Department of Physics, Graduate School of Science, Kyoto University, Kyoto 606-8502, Japan*

December 22, 2018

Abstract

Important features of low-frequency collective vibrational excitations in neutron drip line nuclei are studied. We emphasize that pairing anti-halo effect in the Hartree-Fock-Bogoliubov (HFB) theory play crucial roles to realize collective motions in loosely bound nuclei. We study the spatial properties of one particle - one hole (1p-1h) states with/without selfconsistent pairing correlations by solving simplified HF(B) equations in coordinate space. Next, by performing Skyrme-HFB plus selfconsistent quasiparticle random phase approximation (QRPA) we investigate the first 2^+ states in neutron rich Ni isotopes. Three types of calculations, HFB plus QRPA, resonant BCS plus QRPA, and RPA are compared.

1 Introduction

The study of the properties of nuclei far from the β -stability line is one of the most active and challenging issues in nuclear structure physics. Especially interesting phenomena concern the loosely bound neutron systems close to the neutron drip line. Low-frequency collective vibrational excitations in neutron drip line nuclei are one of the most interesting subjects. Naively we expect low-frequency vibrational modes associated with low-density neutron matter (neutron skin and halo). A famous one is soft dipole mode [1, 2]. However it is a fundamental question whether such collective modes can really appear or not.

Vibrational excitations are represented as coherent superposition of 1p-1h states. In stable nuclei, because the Fermi energies are deep, 1p-1h states between tightly bound single-particle states having similar spatial characters only contribute, and these 1p-1h states concentrate around the nuclear surface. Around neutron drip line, by contrast, 1p-1h states between tightly bound, loosely bound, resonance, and non-resonant continuum states, contribute. Because each single-particle state has different spatial extent, 1p-1h states among them have different spatial characters. Therefore it is a non-trivial problem whether vibrational modes can be realized as a result of coherency between such 1p-1h states.

In Section 2 we examine spatial properties of 1p-1h states in neutron drip line nuclei. First we study characters of 1p-1h states without pairing correlations by solving the Woods-Saxon potential. Next, by solving simplified HFB equation in coordinate space, we emphasize that selfconsistent pairing correlations play important roles to realize collective motions in neutron drip line nuclei. In Sec.3 we perform Skyrme-HFB plus QRPA calculations for the first 2^+ states in neutron rich Ni isotopes. By comparing three types of calculations, HFB plus QRPA, resonant BCS plus QRPA, and RPA, we show that selfconsistent pairing correlations play important roles to realize low-frequency collective vibrational excitations in neutron drip line nuclei.

2 1p-1h states in neutron drip line nuclei

2.1 1p-1h states without pairing correlations

We consider the spatial localization of 1p-1h states as an important condition for collective vibrational motions. Before studying 1p-1h states in neutron drip line region, we examine neutron 1p-1h states in ^{208}Pb as a typical example of stable nuclei for comparison. Because the Fermi energy is about -8 MeV, all wave functions around Fermi energy are tightly bound and spatially localized as shown in Fig.1. These wave functions are provided by solving the Woods-Saxon potential. The remarkable point is that all

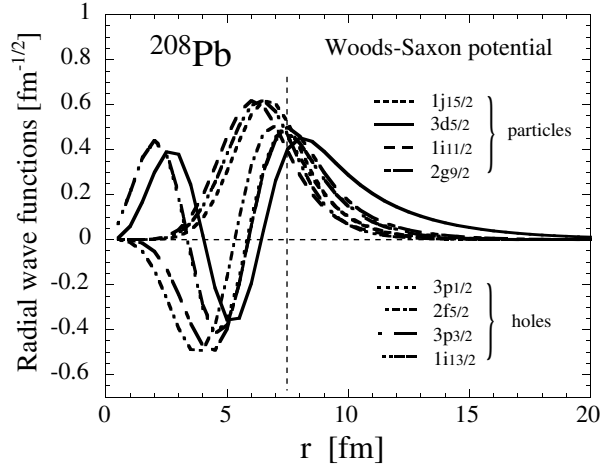


Figure 1: The neutron radial wave functions around Fermi energy in ^{208}Pb .

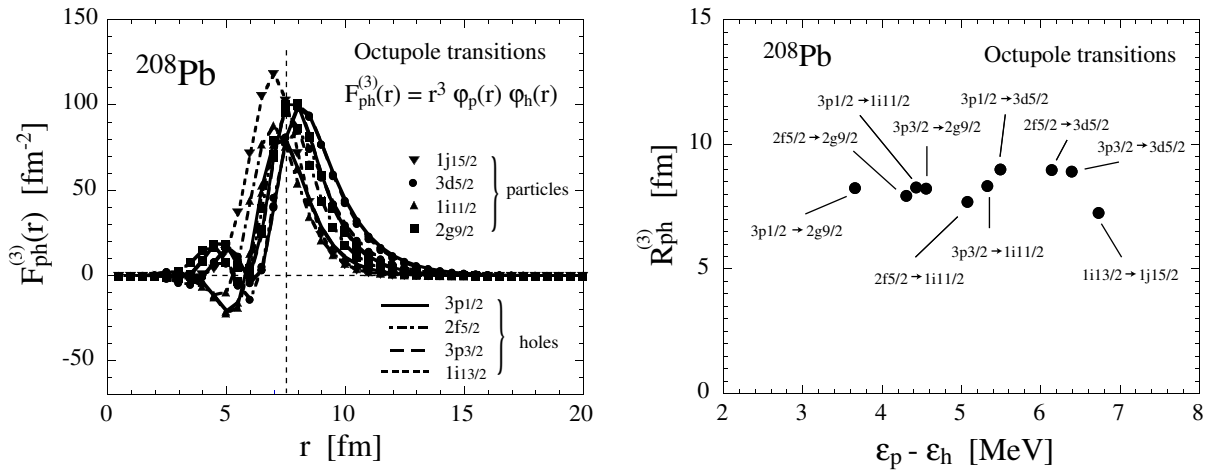


Figure 2: The spatial distributions of 1p-1h states $F_{ph}^{(3)}(r)$ for octupole transitions and the corresponding radii $R_{ph}^{(3)}$ in ^{208}Pb are shown as a function of particle-hole energies $\varepsilon_p - \varepsilon_h$.

wave functions have large overlaps around the surface region. We define the spatial distributions of 1p-1h states as

$$F_{ph}^{(L)}(r) \equiv \varphi_p(r) \cdot r^L \cdot \varphi_h(r), \quad (1)$$

where L is multipolarity of the transition and φ_p (φ_h) are radial wave functions of particle (hole) states. The spatial integration of $F_{ph}^{(L)}(r)$ gives the radial part of the particle-hole transition matrix element $\langle p | r^L | h \rangle = \int dr F_{ph}^{(L)}(r)$. In Fig.2, $F_{ph}^{(L)}(r)$ for octupole transitions are plotted. The hole (particle) states are indicated by lines (symbols), and each combination of a line and a symbol represents a 1p-1h configuration. As seen, all 1p-1h states are localized around the surface region. This feature is an important condition for realization of collective motions, and this condition is satisfied in stable nuclei. For further discussion, we define the "radii" of 1p-1h states $R_{ph}^{(L)}$ as the second moment of $F_{ph}^{(L)}(r)$,

$$R_{ph}^{(L)} \equiv \left\{ \frac{\int dr r^2 F_{ph}^{(L)}(r)}{\int dr F_{ph}^{(L)}(r)} \right\}^{1/2}. \quad (2)$$

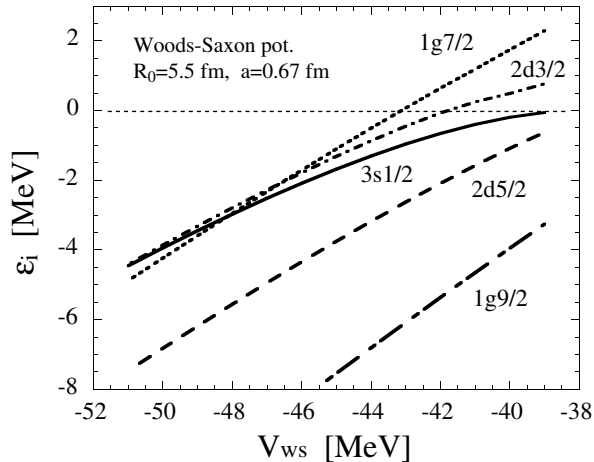


Figure 3: The neutron single-particle energies around ^{86}Ni are plotted as a function of the depth V_{WS} . $V_{WS} \approx -41$ MeV corresponds to ^{86}Ni .

In Fig.2, $R_{ph}^{(3)}$ are plotted as a function of particle-hole energies $\varepsilon_p - \varepsilon_h$. All $R_{ph}^{(3)}$ concentrate around the surface region in stable nuclei.

Next we investigate how the distributions of $R_{ph}^{(L)}$ change around neutron drip line region. We consider neutron rich Ni isotopes as a typical example. In the Hartree-Fock (HF) calculation with Skyrme SLy4 parameter, ^{86}Ni is the neutron drip line nucleus. By taking into account pairing correlations, more neutrons can bound. However the precise position of the neutron drip line depends on the treatment of pairing correlations. For example, the drip line nucleus is ^{88}Ni in Ref.[3] and ^{92}Ni in Ref.[4]. The predicted drip line also depends on the effective interactions and the frameworks, i.e., relativistic or non-relativistic approaches (for example,[4, 5]). In the present study we consider up to ^{88}Ni for further discussion, because our purpose is to investigate the qualitative aspects of vibrational excitations in neutron drip line nuclei.

In Fig.3 the neutron single-particle energies around ^{86}Ni are shown as a function of the depth V_{WS} of the Woods-Saxon potential. $V_{WS} \approx -41$ MeV corresponds to the single-particle energies in ^{86}Ni calculated by HF with SLy4. We consider 1p-1h states of quadrupole transitions around loosely bound $3s_{1/2}$ state (the Fermi level). The resonant states, $2d_{3/2}$ and $1g_{7/2}$, are particle states. In Fig.4 the radii of single-particle levels R_i are shown. The radii of bound states with large- ℓ , $1g_{9/2}$ and $2d_{5/2}$, don't change as approaching the drip line. On the other hand, the radius of $3s_{1/2}$ state becomes rapidly large in the limit of zero binding energy, i.e., neutron halo. Concerning particle states, $2d_{3/2}$ and $1g_{7/2}$, while the single-particle energies are negative, these radii change slowly as a function of V_{WS} . On the other hand, once the single-particle energies become positive (resonant states), the radii increase suddenly. In Fig.4 the radii of 1p-1h states R_{ph} for quadrupole transitions are plotted as a function of V_{WS} . The hole (particle) states are indicated by lines (symbols). Up to $V_{WS} \leq -44$ MeV, corresponding to stable nuclei region, all R_{ph} are localized around the surface region. By contrast, in the drip line region $V_{WS} \geq -44$ MeV, R_{ph} strongly depend on the particle-hole configurations. Size of R_{ph} is mainly determined by the spatial extent of hole wave functions. The localization of 1p-1h states becomes more sparse and the condition for realization of collective motions is not satisfied as approaching the drip line. We may conclude that neutron drip line region is under the situation that collective motions are suppressed and single-particle like excitations appear dominantly. In next subsection we discuss how this situation is significantly modified by including selfconsistent pairing correlations.

2.2 Roles of selfconsistent pairing correlations

It is a well-known fact that pairing correlations are important ingredient to describe collective vibrational excitations. In this study we want to emphasize that selfconsistent pairing correlations described in the HFB theory play important roles in neutron drip line nuclei in non-trivial ways.

Pairing anti-halo effect [6] is an important property of the HFB theory, and qualitatively modifies the asymptotic behavior of the quasiparticle wave functions. In HF the asymptotic behavior of the bound

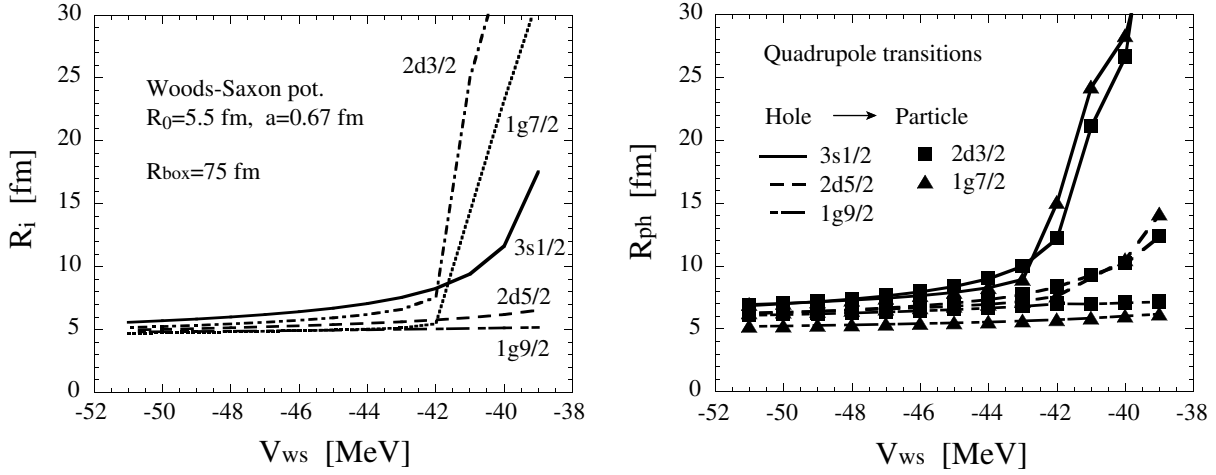


Figure 4: The radii of neutron single-particle levels R_i and the radii of 1p-1h states R_{ph} for quadrupole transitions around ^{86}Ni as a function of the depth V_{WS} .

states wave functions ($\varepsilon_{lj,n} < 0$) for $r \rightarrow \infty$ is

$$\varphi_{lj}^{HF}(\varepsilon_{lj,n}, r) \rightarrow \exp(-\alpha_{lj,n} r), \quad (3)$$

where $\alpha_{lj,n} = \sqrt{-2m\varepsilon_{lj,n}}/\hbar$. The decay constant $\alpha_{lj,n}$ can approach zero for $\varepsilon_{lj,n} \rightarrow 0$. For positive energy states ($\varepsilon > 0$),

$$\varphi_{lj}^{HF}(\varepsilon, r) \rightarrow C_{lj} [\cos(\delta_{lj}) r j_l(\beta r) - \sin(\delta_{lj}) r n_l(\beta r)] \quad (4)$$

where $\beta = \sqrt{2m\varepsilon}/\hbar$. j_l and n_l are spherical Bessel and Neumann functions, and δ_{lj} is the phase shift corresponding to the angular momentum (lj).

By taking into account pairing correlations, irrespective of selfconsistent or non-selfconsistent pairing, quasiparticle wave functions have two components, hole wave functions $v_{lj}(r)$ and particle wave functions $u_{lj}(r)$. In HF plus BCS calculations both $v_{lj}(r)$ and $u_{lj}(r)$ are just proportional to HF single-particle wave functions,

$$\begin{aligned} u_{lj}(\varepsilon_{lj,n}, r) &= u_{lj,n} \varphi_{lj}^{HF}(\varepsilon_{lj,n}, r) \\ v_{lj}(\varepsilon_{lj,n}, r) &= v_{lj,n} \varphi_{lj}^{HF}(\varepsilon_{lj,n}, r), \end{aligned} \quad (5)$$

where $v_{lj,n}$ ($u_{lj,n}$) are occupation (unoccupation) amplitudes. Therefore both hole and particle wave functions have the same asymptotic behavior for $r \rightarrow \infty$. Eqs.(5) are usually defined only for bound states. Recently the HF plus resonant BCS method was proposed [7, 8]. In this approach resonant states are take into account for particle states. Applicability of the resonant BCS method for ground state properties is discussed in Ref.[3]. In HFB, by contrast, the asymptotic behavior of the quasiparticle wave functions is qualitatively different. We examine the HFB equation in coordinate space [9, 10, 11],

$$\begin{pmatrix} h_{lj}(r) - \lambda & \Delta(r) \\ \Delta(r) & -h_{lj}(r) + \lambda \end{pmatrix} \begin{pmatrix} u_{lj}(E_{qp}, r) \\ v_{lj}(E_{qp}, r) \end{pmatrix} = E_{qp} \begin{pmatrix} u_{lj}(E_{qp}, r) \\ v_{lj}(E_{qp}, r) \end{pmatrix}, \quad (6)$$

where $h_{lj}(r)$ and $\Delta_{lj}(r)$ are the mean field and the pairing field respectively. For the discrete region $(E_{qp} + \lambda) < 0$, both hole and particle wave functions decay exponentially at infinity,

$$\begin{aligned} u_{lj}(E_{lj,n}, r) &\rightarrow \exp(-\alpha_{lj,n}^{(1)} r) \\ v_{lj}(E_{lj,n}, r) &\rightarrow \exp(-\beta_{lj,n}^{(1)} r) \end{aligned} \quad (7)$$

where $\alpha_{lj,n}^{(1)} = \sqrt{-2m(E_{lj,n} + \lambda)}/\hbar$ and $\beta_{lj,n}^{(1)} = \sqrt{2m(E_{lj,n} - \lambda)}/\hbar$. For the continuum region $(E_{qp} + \lambda) > 0$,

$$\begin{aligned} u_{lj}(E, r) &\rightarrow C_{lj} [\cos(\delta_{lj}) r j_l(\alpha^{(2)} r) - \sin(\delta_{lj}) r n_l(\alpha^{(2)} r)] \\ v_{lj}(E, r) &\rightarrow \exp(-\beta^{(2)} r) \end{aligned} \quad (8)$$

where $\alpha^{(2)} = \sqrt{2m(E + \lambda)}/\hbar$ and $\beta^{(2)} = \sqrt{2m(E - \lambda)}/\hbar$. The hole wave functions always decay exponentially. The minimum value of the decay constant β is estimated as following. If a discrete quasiparticle state with minimum energy E_μ is present, the minimum value of the decay constant becomes $\beta_\mu^{(1)} = \sqrt{2m(E_\mu - \lambda)}/\hbar$. The HFB quasiparticle energies E_μ are well approximated by the canonical quasiparticle energies [12], $E_\mu \simeq E_\mu^{can} \equiv \sqrt{(\epsilon_\mu^{can} - \lambda)^2 + (\Delta_\mu^{can})^2}$, where ϵ_μ^{can} and Δ_μ^{can} are the canonical single-particle energy and the canonical pairing gap. This means that $\beta_\mu^{(1)}$ stays at finite value

$$\beta_\mu^{(1)} \rightarrow \sqrt{2mE_\mu}/\hbar \geq \sqrt{2m\Delta_\mu^{can}}/\hbar > 0 \quad (9)$$

with finite Δ_μ^{can} for $\lambda \rightarrow 0$. Selfconsistent pairing correlations affect the asymptotic behavior of all hole wave functions, and especially act against a development of an infinite rms radius that characterizes the wave functions of s and p states in the limit of vanishing binding energy. We call this localization of hole wave functions "pairing anti-halo effect". Though this terminology was used for the localization of the normal density distribution $\rho(r)$ in Ref.[6], the microscopic mechanism is the same. In neutron drip line region where discrete HFB solutions don't exist, the analysis is more complicated. However, as numerically shown in Ref.[6], pairing anti-halo effect plays the roles to localize hole wave functions in similar way.

We solve the coordinate space HFB equation Eq.(6) with box boundary conditions $R_{box} = 30$ fm. For the HF potential the Woods-Saxon potential is used. The pairing potential is selfconsistently derived by the density dependent pairing interaction,

$$V_{pair}(\mathbf{r}, \mathbf{r}') = V_{pair} \left[1 - \frac{\rho(\mathbf{r})}{\rho_c} \right] \delta(\mathbf{r} - \mathbf{r}'). \quad (10)$$

The parameters are $V_{pair} = -350$ MeV fm⁻³ and $\rho_c = 0.16/2$ fm⁻³ with the cut-off energy $E_{cut} = 50$ MeV. ρ_c is taken to be the half of the saturation density, because Eq.(6) is solved only for neutrons. This pairing parameter set gives the averaged pairing gap $\bar{\Delta} \approx 1.5$ MeV in the region -51 MeV $< V_{WS} < -39$ MeV. The average pairing gap is defined as the integral of the pairing field with the abnormal density $\tilde{\rho}(\vec{r})$,

$$\bar{\Delta} = \frac{\int d\vec{r} \tilde{\rho}(\vec{r}) \Delta(\vec{r})}{\int d\vec{r} \tilde{\rho}(\vec{r})}. \quad (11)$$

In Fig.5, the radii of hole wave functions around ⁸⁶Ni provided by HFB calculations are plotted. By comparing the radii of the single-particle states without selfconsistent pairing correlations (HF and HF plus resonant BCS in Fig.4), the spatial distributions of the hole wave functions are completely different. Due to pairing anti-halo effect, the radii in HFB spatially concentrate around the surface region.

We consider how spatial characters of 1p-1h states are modified by taking into account selfconsistent pairing correlations. First of all, by including pairing correlations, irrespective of selfconsistent or non-selfconsistent, the possible 1p-1h configurations increase considerably, i.e., not only particle-hole but also particle-particle and hole-hole configurations can contribute. We define a spatial distribution of 1p-1h state from a hole part $v_{lj}(E)$ to a particle part $u_{l'j'}(E')$,

$$F^{(L)}[u_{l'j'}(E'), v_{lj}(E)](r) \equiv u_{l'j'}(E', r) \cdot r^L \cdot v_{lj}(E, r), \quad (12)$$

and the radius,

$$R^{(L)}[u_{l'j'}(E'), v_{lj}(E)] \equiv \left\{ \frac{\int dr r^2 F^{(L)}[u_{l'j'}(E'), v_{lj}(E)](r)}{\int dr F^{(L)}[u_{l'j'}(E'), v_{lj}(E)](r)} \right\}^{1/2}. \quad (13)$$

We use shorthand notations $F_{uv}^{(L)}(r)$ and $R_{uv}^{(L)}$, unless these don't cause confusions. In Fig.5 the radii $R_{uv}^{(2)}$ in HFB are plotted. As we have mentioned in subsec.2.1, the radii of 1p-1h states are mainly determined by the spatial extent of hole states. Because the radii R_v in HFB are localized due to the pairing anti-halo effect, the radii R_{uv} in HFB concentrate around the surface region. This localization of R_{uv} can happen by treating pairing correlation selfconsistently. In resonant BCS, such localization can not appear. Generally speaking, the spatial distribution of particle-particle configurations between resonant states are always far outside from the surface region in resonant BCS.

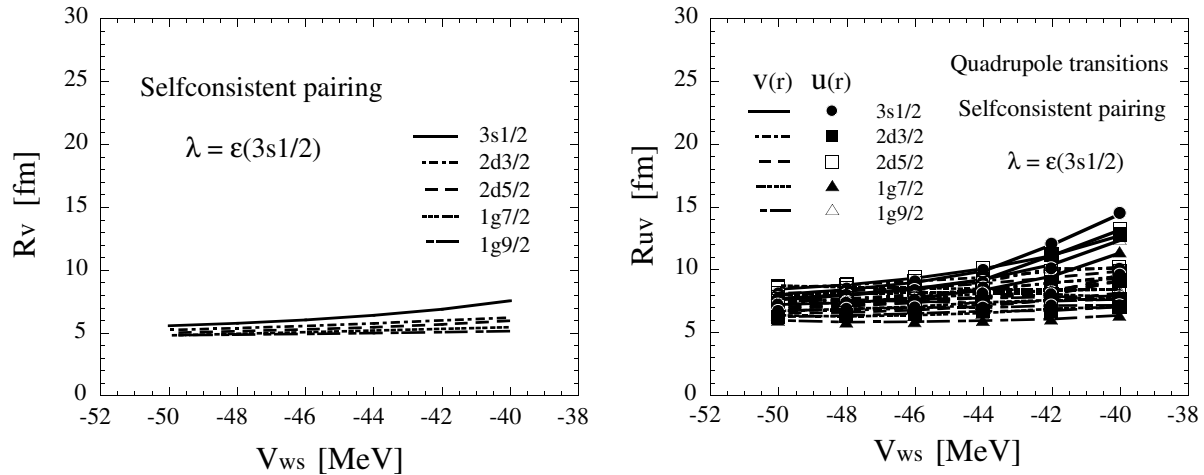


Figure 5: The radii of hole wave functions R_v and the radii of 1p-1h states R_{uv} in HFB around ^{86}Ni as a function of the depth V_{WS} .

3 HFB plus QRPA calculations

3.1 Formulation

We consider the first 2^+ states in neutron rich Ni isotopes by Skyrme-HFB plus selfconsistent QRPA calculations. By selfconsistent we mean that the HFB mean fields are determined selfconsistently from an effective force and the residual interaction of the QRPA problem is derived from the same force. The QRPA problem is solved by the response function method in coordinate space. A detailed account of the method can be found in Ref.[13, 14, 15]. Here, we just recall the main steps of the calculation. The QRPA Green's function \mathbf{G} is a solution of a Bethe-Salpeter equation,

$$\mathbf{G} = \mathbf{G}_0 + \mathbf{G}_0 \mathbf{V} \mathbf{G} . \quad (14)$$

The knowledge of \mathbf{G} allows one to construct the response function of the system to a general external field, and the strength distribution of the transition operator corresponding to the chosen field is just proportional to the imaginary part of the response function. The residual interaction \mathbf{V} between quasiparticles is derived from the Hamiltonian density $\langle H \rangle$ of Skyrme interaction by the so-called Landau procedure,

$$V_{\alpha\beta} = \frac{\partial^2 \langle H \rangle}{\partial \rho_\beta \partial \rho_{\bar{\alpha}}} . \quad (15)$$

The index α ($\alpha = 1, 2, 3$) stands for particle-hole (ph), particle-particle (pp), and hole-hole (hh) channels. The notation $\bar{\alpha}$ means that whenever α is pp (hh) then $\bar{\alpha}$ is hh (pp). The residual interaction \mathbf{V} has an explicit momentum dependence,

$$\mathbf{V}(\mathbf{r}, \mathbf{r}') = \mathbf{F}[\vec{\Delta}_U + \vec{\Delta}_V, \vec{\Delta}_U + \vec{\Delta}_V, \vec{\nabla}_U \pm \vec{\nabla}_V, \vec{\nabla}_U \pm \vec{\nabla}_V] \delta(\mathbf{r} - \mathbf{r}') . \quad (16)$$

The explicit form of the form factor \mathbf{F} is shown in Ref.[13]. These momentum dependence are explicitly treated in our calculation. Because we calculate only natural parity (non spin-flip) excitations, we drop the spin-spin part of the residual interaction. The Coulomb and spin-orbit residual interactions are also dropped.

The ground states are given by Skyrme-HFB calculations. The HFB equation is diagonalized on a Skyrme-HF basis calculated in coordinate space with box boundary conditions $R_{box} = 20$ fm. Spherical symmetry is imposed on quasiparticle wave functions. The quasiparticle cut-off energy is taken to be $E_{cut} = 50$ MeV, and the angular momentum cut-off is $\ell_{max} = 7\hbar$ in our HFB and QRPA calculations. The Skyrme parameter SLy4 [16] are used for the HF mean-field, and the density-dependent, zero-range pairing interaction Eq.(10) is adopted for the pairing field. The parameters are $V_{pair} = -555$ MeV fm $^{-3}$, $\rho_c = 0.16$ fm $^{-3}$, so as to give the average neutron pairing gap $\bar{\Delta}_n \approx 12/\sqrt{A}$ in ^{86}Ni .

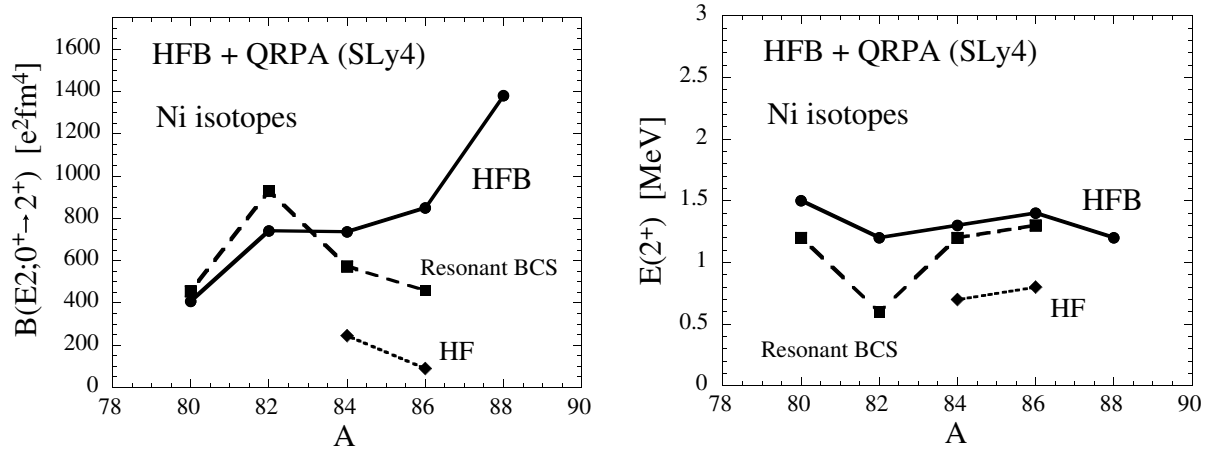


Figure 6: The $B(E2, 0_1^+ \rightarrow 2_1^+)$ values and the excitation energies of the first 2^+ states in neutron rich Ni isotopes calculated by HFB plus selfconsistent QRPA, resonant BCS plus QRPA, and RPA with Skyrme SLy4 force.

3.2 Ni isotopes

In order to emphasize the importance of pairing anti-halo effect for realization of collective vibrational excitations, we compare three types of calculations, HFB plus QRPA, resonant BCS plus QRPA (no pairing anti-halo effect), and RPA (no pairing) for the first 2^+ states in neutron rich Ni isotopes. In Fig.6 the $B(E2, 0_1^+ \rightarrow 2_1^+)$ values and excitation energies of the first 2^+ states in neutron rich Ni isotopes up to ^{88}Ni in HFB plus QRPA, and ^{86}Ni for resonant BCS plus QRPA corresponding the neutron drip line are shown. To construct the quasiparticle wave functions without pairing anti-halo effect, we perform resonant BCS calculations. In resonant BCS calculations for the ground states, we include resonant states (localized states) for particle states. To identify the resonant states in calculations with box boundary conditions $R_{box} = 20$ fm, we introduced an additional cut-off radius $R_{BCS} = 10$ fm and the single-particle orbits having the radii less than R_{BCS} are taken into account for the pairing problems of the ground states. The resonant $1g_{7/2}$ and $2d_{3/2}$ states are included. The orbits with the radii larger than R_{BCS} are included only for QRPA model space. Because we intend qualitative discussion of microscopic aspects of vibrational excitations, we performed constant- Δ BCS calculations to avoid technical complexities that are inherent in non-selfconsistent calculations (lack of selfconsistency in the pairing potential, different energy cut-off scheme for HF plus resonant BCS calculations $E_{cut} = 5$ MeV and QRPA calculations $E_{cut} = 50$ MeV, and neglecting the contribution of non-resonant continuum state that plays important roles in pairing correlations in neutron drip line nuclei [6, 17, 18]). The constant pairing gap $\Delta = 0.8$ MeV is chosen to reproduce low-lying quasiparticle energies in Skyrme-HFB calculations. We have checked the sensitivity of the pairing gap parameter, and the calculated excitation energies and the $B(E2)$ values are qualitatively the same. For the residual interaction we used the exactly same interaction in HFB plus QRPA calculations.

From ^{80}Ni to ^{82}Ni , HFB plus QRPA and resonant BCS plus QRPA calculations give qualitatively similar results. The energies decrease and the $B(E2)$ values increase. On the other hand, as approaching the neutron drip line, the calculated $B(E2)$ values exhibit different behavior. In HFB plus QRPA calculations the $B(E2)$ values increase monotonically. On the other hand, the $B(E2)$ values suddenly decrease from ^{82}Ni to ^{86}Ni in resonant BCS plus QRPA. The main qualitative difference between HFB plus QRPA and resonant BCS plus QRPA is the presence of pairing anti-halo effect. In resonant BCS, due to lack of pairing anti-halo effect, particle-particle configurations between resonant states, $1g_{7/2}$ and $2d_{3/2}$, and also particle-hole configurations with hole $3s_{1/2}$ state are spatially decoupled to the other 1p-1h states, and can not participate in the collective excitations. The results of HF plus RPA calculations for ^{84}Ni and ^{86}Ni are also shown. These excitations have single-particle like characters, and the excitation energies are almost the same with specific 1p-1h energies ($2d_{5/2} \rightarrow 3s_{1/2}$ in ^{84}Ni and $3s_{1/2} \rightarrow 2d_{3/2}$ in ^{86}Ni). The $B(E2)$ values in resonant BCS plus QRPA are larger than the values in HF plus RPA, because hole-hole configurations can contribute to make the collective modes in resonant BCS plus QRPA

calculations.

For another example that indicates the importance of selfconsistent pairing correlations, we have shown that neutron pairing correlations play important roles to explain the experimentally observed anomalously large $B(E2)$ values in neutron rich nuclei, ^{32}Mg and ^{30}Ne [13]. This is an actual example that pairing anti-halo effect plays important roles to realize collective motions in neutron drip line region.

4 Conclusion

We discussed the important microscopic aspects of low-frequency collective vibrational excitations in neutron drip line nuclei. We emphasized that pairing anti-halo effect in the HFB theory plays important roles to realize collective motions in loosely bound nuclei. We performed Skyrme-HFB plus selfconsistent QRPA calculations for the first 2^+ states in neutron rich Ni isotopes. By comparing three types of calculations, HFB plus QRPA, resonant BCS plus QRPA, and RPA, the importance of pairing anti-halo effect was shown in realistic calculations.

5 ACKNOWLEDGMENTS

We acknowledge Professor K. Matsuyanagi for valuable discussions. Numerical computation in this work was carried out at the Yukawa Institute Computer Facility.

References

- [1] P. G. Hansen, and B. Jonson, *Europhys. Lett.* **4**, 409 (1987).
- [2] K. Ikeda, *Nucl. Phys.* **A538**, 355c (1992).
- [3] M. Grasso, N. Sandulescu, Nguyen Van Giai, and R. J. Liotta, *Phys. Rev. C* **64**, 064321 (2001).
- [4] S. Mizutori, J. Dobaczewski, G. A. Lalazissis, W. Nazarewicz, and P. -G. Reinhard, *Phys. Rev. C* **61**, 044326 (2000).
- [5] J. Meng, *Phys. Rev. C* **57**, 1229 (1998).
- [6] K. Bennaceur, J. Dobaczewski, and M. Ploszajczak, *Phys. Lett. B* **496**, 154 (2000).
- [7] N. Sandulescu, R. J. Liotta, and R. Wyss, *Phys. Lett. B* **394**, 6 (1997).
- [8] N. Sandulescu, Nguyen Van Giai, and R. J. Liotta, *Phys. Rev. C* **61**, 061301 (2000).
- [9] A. Bulgac, preprint No. FT-194-1980, Institute of Atomic Physics, Bucharest, 1980, (nucl-th/9907088).
- [10] J. Dobaczewski, H. Flocard, and J. Treiner, *Nucl. Phys.* **A422**, 103 (1984).
- [11] S. T. Belyaev, A. V. Smirnov, S. V. Tolokonnikov, and S. A. Fayans, *Yad. Fiz.* **45**, 1263 (1987).
- [12] J. Dobaczewski, W. Nazarewicz, T. R. Werner, J. F. Berger, C. R. Chinn, and J. Decharge, *Phys. Rev. C* **53**, 2809 (1996).
- [13] M. Yamagami, and Nguyen Van Giai, *Phys. Rev. C* **69**, 034301 (2004).
- [14] M. Yamagami, E. Khan, and Nguyen Van Giai, in *Proceedings of the International Symposium on Frontiers of Collective Motions 2002, University of Aizu, Japan*, edited by H. Sagawa and H. Iwasaki (World Scientific, Singapore, 2003), p.230.
- [15] E. Khan, N. Sandulescu, M. Grasso, and Nguyen Van Giai, *Phys. Rev. C* **66**, 024309 (2002).
- [16] E. Chabanat, P. Bonche, P. Haensel, J. Meyer, and R. Schaeffer *Nucl. Phys.* **A635**, 231 (1998); Erratum *Nucl. Phys.* **A643**, 441 (1998).
- [17] K. Bennaceur, J. Dobaczewski, and M. Ploszajczak, *Phys. Rev. C* **60**, 034308 (1999).
- [18] I. Hamamoto, and B. R. Mottelson, *Phys. Rev. C* **68**, 034312 (2003).